Sixth International Conference on Durability of Concrete Structures **Paper Number MID07**
18 - 20 July 2018
University of Leeds, Leeds, West Yorkshire, LS2 9JT, United Kingdom

A Novel Methodology of Powder-based Cementitious Materials in 3D Inkjet Printing for Construction Applications

P. Shakor and S. Nejadi
Centre for Built Infrastructure Research, School of Civil and Environmental,
Faculty of Engineering and Information Technology, University of Technology Sydney, Australia.

G. Paul
Centre for Autonomous Systems, School of Electrical, Mechanical and Mechatronics,
Faculty of Engineering and Information Technology, University of Technology Sydney, Australia.

J. Sanjayan
Centre for Sustainable Infrastructure, School of Engineering, Civil and Construction,
Faculty of Science, Engineering & Technology, Swinburne University of Technology, Hawthorn, Australia.

ABSTRACT

Recently, additive manufacturing techniques such as 3D printing are becoming increasingly popular and widely used in a variety of applications. Inkjet 3D printing (i.e. powder-based printing) is one of the most reliable frequently-implemented techniques in 3D printers. This paper discusses a novel methodology to replace the currently used typical powders in 3D printing to make it possible to use the printed specimens in construction applications. The printed cubic (20×20×20mm) and prism (60×5×5mm) specimens with different saturation levels are printed to investigate the relative strength of the 3D printed specimens. Curing in different saturation environments can increase their strength and durability. In general, the experimental results show that the highest compressive strength was recorded (14.68MPa) for the samples that are first cured in water then dried in an oven for one hour at 40ºC, comparing to the samples that are cured without drying at 40ºC (4.81MPa). Accordingly, it has been discovered that the post-processing technique has an effective and significant impact on the strength of the printed specimens. Furthermore, samples which are cast using manual mixing have been also been compared in detail.

Keywords: 3D printing, cementitious materials, calcium aluminate cement, post-processing, compressive and flexural strength.

1.0 INTRODUCTION

Currently, 3D printing technology has been developed for different purposes, in particular, it has been employed in food preparation, medicine/healthcare and various industry applications (Castaneda *et al.* 2015; Wegrzyn *et al.* 2012). It is recognized that this technology could entirely change a range of production approaches (Lipson & Kurman 2013). The principal benefit of 3D printing technologies is that we can directly construct parts in one step from the CAD data (Vaezi & Chua 2011). 3D printing could reduce 35-60% of the overall costs of concrete construction due to the removal of formwork (Lloret *et al.* 2015). Nowadays, 3D printing is being utilised for construction purposes by employing both approaches: powder-based, and extrusion printing (Shakor *et al.* 2017).

There are few studies into the simultaneous use of both approaches since there are many limitations that need to be overcome in order to make them more applicable in construction. Inkjet printing is, however, commonly used for biological, medical and biochemical purposes (Zhou *et al.* 2014). The purpose of this study to investigate the modification of the printer's deposition material to a cementitious powder which can be utilized for construction purposes. The original powder is a mixture of plaster powder which has been used in the inkjet 3D printer (Zprinter 150). The ingredients were selected as a vinyl polymer, plaster and carbohydrate (3DSystems 2012; Feng, *et al.*, 2015; Feng, 2015a).

The Inkjet printing (3D printer) is the technique that has been utilized in this paper to produce structural components. The nozzle of the 3DP printer sprays the binder which consists of humectant and water (Farzadi *et al.* 2014; Farzadi *et al.* 2015). The printed specimen was created through layer-by-layer printed powder and using a binder which bound layers together. This process continues until the samples are complete. Currently, the 3DP method is able to print numerous products using different powders like

sand, plaster, cement, metal, and ceramic (Buswell *et al.* 2007; Michele & Emanuel 2003). Recently, the most appropriate materials for printed structural elements is a mortar mixed cementitious material (e.g. cementitious concrete composed of cement and sand) to produce civil engineering components. This paper focuses on the inkjet printing use in construction applications and the approaches to modifying the powder in the printer. Further, it has been discussed how to increase the strength of the specimen using different curing conditions.

2.0 MATERIALS AND METHODS

2.1 Material composition

The Z-printer powder consists of plaster, vinyl polymer and carbohydrate. D10, D50, and D90 values, which are representative of the mean particle size for 10%, 50%, and 90% of the materials, respectively, were obtained using a laser to measure which is equal to 1.48, 23.07 and 70.12 µm, respectively. The particle size distribution of powder in the 3D printer (Z-printer150, Z-Corporation, USA) employs a method such as particle size analyser (Cilas 1190). The specific surface area of Z-powder has been found to be 0.999 $m^2.g^{-1}$ when tested by (BELSORP-max).

The three basic materials used in this study are ordinary Portland cement (OPC) (Geelong cement), calcium aluminate cement (CAC) (CIMENT FONDU, Kerneos) and fine sand (TGS Industrial Sands Pty. Ltd., Australia - maximum size of approximately 300 µm). Portland cement is a conventional cement type that is widely used, and it consists of calcium, silica, alumina and iron. CAC is another type of cement comprising hydraulic calcium aluminates. It is also known as “aluminous cement" and "high-alumina cement". This type of cement is utilised in specialised applications (e.g. emergency repairs and foundation construction).

Particle size distributions for 10%, 50% and 90% of CAC (passed through 150 µm sieves) which are 3.38, 79.93 and 127.11 µm, for OPC are 0.19, 8.93 and 38.46 µm, respectively. The sieve is performed for CAC between 75 and 150 µm. The bulk particle densities for CAC and OPC are 1.23 and 0.92 $g.cm^{-3}$ respectively while the specific surface area for the mixture of both types of cement is 1.021 $m^2.g^{-1}$, which is conducted by (BELSORP-max) as shown in Table 1. The mixed ratio contains 67.8% CAC and 32.2% OPC. Note that the proportion of CAC is higher due to the similarity of their particle size being closer to Z-powder. For comparison purposes, 4.5% of the total mix from lithium carbonate (lithium carbonate, reagent grade, ACS) is poured into the mix, which is used as an agent to accelerate the setting time of the cement (Lin *et al.* 2015). It can produce rapid setting, high early strength, excellent adhesion and stability.

Table 1. Powder properties for starting Z-powder and CAC & OPC materials

Powder properties	Z-powder	CAC & OPC powder 67.8 : 32.2
D10 (µm)	1.480	1.010
D50 (µm)	32.07	14.46
D90 (µm)	70.12	56.92
Bulk particle density ($g.cm^{-3}$)	0.912	1.023
Specific surface area ($m^2.g^{-1}$)	0.999	1.021

The CAC was sieved by 150 to 75 µm mesh sieves and shaken for about 5 minutes. Then it was blended with OPC using a Hobart mixer; lithium carbonate was added and in some mixes, a further 5% of fine sand was also added. Then, the mixer was operated at the rotation speed of 1450 rpm for 10 minutes. Since the CAC and OPC powders have different particle size distributions (i.e. OPC is finer than CAC), these two types of cement powders were mixed to obtain one powder with a similar allocation as the target powder, which is used in the Z-printer.
A fluid solution (Zb® 63, Z-Corp, USA) was used as an adhesive during the 3DP process. This fluid is known as a binder. It has a commercial clear liquid solution with a viscosity close to pure water. The formation of the binder was mostly water with 2-Pyrrolidone (Farzadi *et al.* 2014).

In this study, a mixture of CAC and OPC was utilized as the powder and Zb63 (containing humectant and water) was used as a binder to build 3D objects.

2.2 Fabrication of Specimens

The specimens were made using a 3D printer Z150 (ZCorporation Inc., USA; now possessed by 3D Systems Inc., USA) onto which is mounted an HP11 (C4810A) printhead exertion as a nozzle head. The 3D printer consisted of a build chamber and a feed chamber. As shown in Fig. 1, the build bin produces the 3D samples and a roller mounted with the print head on the gantry spreads the powder to create the 3D sample's layer by layer. The feed bin is filled entirely with powder. Then, the printer nozzle moves and drops the binder (liquid) onto the powder at certain locations to make the samples layer by layer and this ultimately creates the sample. The container of a 3D printer is filled with the mixture powder of CAC and OPC. In order to allow powders derived from the feed bin, the roller spreads a new layer on the bedded layers in the build bin. The build bin will move downward by the thickness of one layer (0.1)mm so that the new layer can be constructed, Fig. 1. When the layer spreads out fully, the nozzle will release the liquid to form an object on the

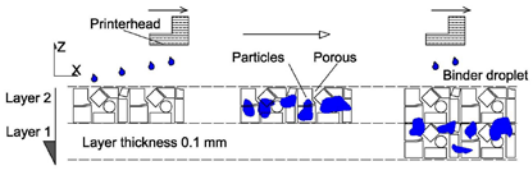

Fig. 1. Layer explanation and powder/binder interaction between layers

bedded powder. These actions will be repeated until the sample is completely constructed.

The 3D inkjet printer could be adjusted for different saturation levels (binder/volume ratio) or the water/cement ratio. The saturation level is defined as the ratio of liquid binder amount to the powder printed bed which is dropped out from the printhead (Miyanaji *et al.* 2016). It is expressed by the following equation (1);

$$Saturation\ level = {}^{Vbinder}/_{Venv.powder} \quad (1)$$

Where the *Vbinder* is known as the volume of binder and the *Venv.powder* is identified as the volume of the powder after it is being rolled on the build chamber of the printer(enveloped powder).

The existing paper represented the relationship between binder/volume ratio in 3DP to water/cement in manual mixing. Currently, new Z-Corps products are used that made it possible to regulate the layers of sample thickness too. The thickness and saturation levels of the specimens had a substantial effect on the porosity and stability of the green parts (referring to a sample that has been removed immediately after it has been printed without post-processing (none cured)) of the specimens. The proper time to remove the specimens from unbounded powder depends on the drying duration times in the printed machine and hydration of cementitious materials. Moreover, the evaporation of the printing liquid plays a key role in the duration of drying samples, as well as porosity which has a major impact on the drying time. Saturation regulation levels in the 3DP can be customised according to the outer and inner scaffold, which are known as the shell and core, respectively.

2.3 Preparation of the specimens

In Fig. 2, cubic specimens (20×20×20)mm and prism specimens (60×5×5)mm were fabricated to measure the compressive strength, flexural strength determine the pore size distribution of the 3D printed powders. Samples were prepared in three primary batches: 1) CAC and OPC with lithium carbonate produced by the 3D printer; 2) CAC, OPC and fine sand produced by the 3D printer and; 3) CAC and OPC with lithium carbonate through hand mixing

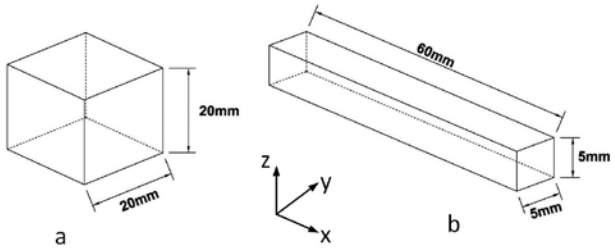

Fig. 2. (a) cubic specimens (20×20×20mm), (b) prism specimens (60×5×5mm).

process (i.e. manual mixing) of mortar mixtures which are detailed in Table 2.

3DP (Z-printer) has the maximum saturation level for the shell and core at 170% and 340%, respectively. The shell saturation level could be inserted between 75%-170% and for the core were between 150% - 340%.

Different ages and different curing conditions were performed for the cubic samples, which were perpendicular to the X-axis and parallel to the Z-

Table 2. Numbers of 3DP cubic specimens at different saturation levels with/without lithium carbonate (Li_2CO_3)

Sample designation	Cementitious mixture	Cured Condition
S75-C75-OW	CAC, OPC	Water
S100-C100-ZN	Zpowder	Non-cure
S100-C100-OW	CAC, OPC	Water
S125-C125-LW	CAC,OPC,Li_2CO_3	Water
S125-C125-OW	CAC,OPC	Water
S150-C150-LW	CAC,OPC,Li_2CO_3	Water
S150-C150-OW	CAC, OPC	Water
S170-C170-OW	CAC, OPC	Water
S75-C150-LW	CAC,OPC,Li_2CO_3	Water
S75-C150-OW	CAC, OPC	Water
S100-C200-LW	CAC,OPC,Li_2CO_3	Water
S100-C200-OW	CAC, OPC	Water
S125-C250-OW	CAC,OPC	Water
S150-C300-LW	CAC,OPC,Li_2CO_3	Water
S150-C300-OW	CAC, OPC	Water
S170-C340-LW	CAC,OPC,Li_2CO_3	Water
S170-C340-OW	CAC, OPC	Water
S170C340-SH	CAC,OPC,Li_2CO_3	Water&$Ca(OH)_2$
W: water cured, N: not cured, L: lithium contain, O: CAC&OPC, Z: Z-powder, S: fine sand, H: cure in $Ca(OH)_2$.		

axis, see Fig. 3. Some of these samples were tested as a green part (none curing). Following this, some of the specimens were cured in water at room temperature for 1, 7 and 28 days.

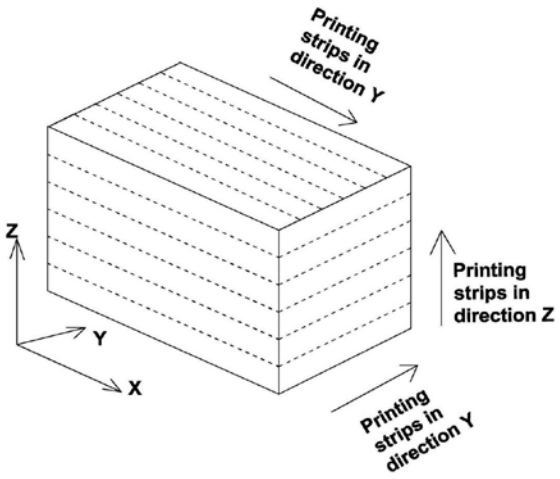

Fig. 3. Directional depiction of the 3D printing process.

According to the AS 1774.5:2014, the porosity tests were conducted for the samples shown in Table 3 and Fig. 4. The experimental tests were prepared in vitro for cubic samples. Consequently, the specimens were dried in an oven (Vtech, XU 225) at 105°C for about 2 hours and then left to cool down to room temperature. The weight of the sample at this stage is designated as dry weight (m_1). Then, samples were put in a bulk density tester (XQK-03), and the air was sucked inside the tester for about 10 min. Next, water was poured into the bucket till it covered the samples completely (about 5 cm in depth), for a period of 10 minutes to ensure that the samples were entirely saturated by water. Then, the weight of the samples in soaking water was measured on the scale (m_2), followed by rolling the four side samples on the damp cloth measured as a (m_3). From this the apparent porosity of cubic samples was calculated using equation (2):

$$Pa = \frac{m3-m1}{m3-m2} x100 \quad (2)$$

3.0 RESULTS & DISCUSSION

3.1 Mechanical properties

The results are shown in Fig. 5, the distribution of the particle size for the Z-powder and substituted powder in the 3D printer (Z-printer150, Z-Corporation, USA) used particle size laser distributor (Cilas1190). According to Asadi-Eydivand *et al.* (2016), the ZP150 powder has a particle size distribution as D10, D50, and D90 are 0.64, 27.36 and 68.83 µm, respectively which is similar to present study. The D10, D50 and D90 represent the range and midpoint of the particle size that is based on sieve analysis results which calculates the act for 10%, 50% and 90% of the mass.

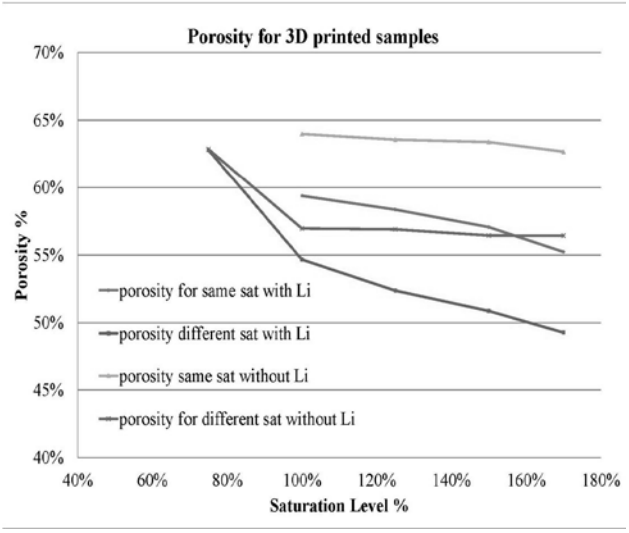

Fig. 4. Porosity at the 3D printed samples

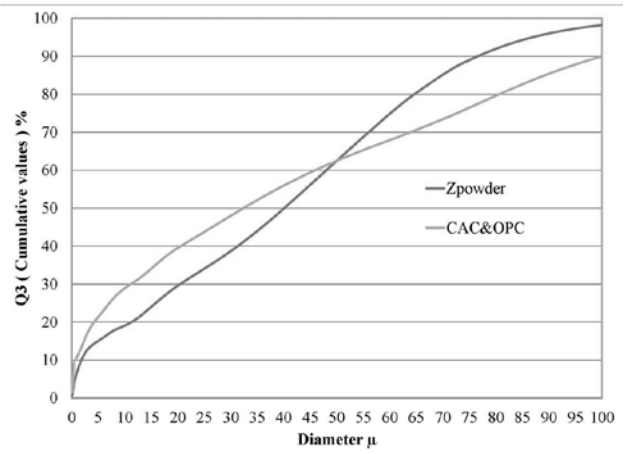

Fig. 5. Particle size distributions for the powders

There are (222) samples in this study consisting of three batches; the first two batches are built via 3D printing, the third and last batches are generated by hand or manual mixing. There is a significant difference between hand mixed and 3D printed specimens due to the different method of creation in 3D printing. The compressive strength of 3D printed samples is weaker than the hand-made mixed specimens as well as having a higher porosity between particles in 3DP.

Table 3. Porosity with different saturation levels of CAC & OPC without Li_2CO_3 analysed by ImageJ.

Sample Name	Porosity %
S100-C200	66.37
S125-C250	65.155
S150-C300	63.64
S170-C340	62.292

The printed specimens are not accurate in dimensions compared with the computer modelled specimens. The standard deviations are between (0.09) to (1.79) mm. These measurements are summarised in Table 4. Results show that most of the samples with greater than 100% saturation levels are oversized. This may be due to unbounded powder that was not completely removed during the de-powdering process, or the samples had swollen due to the higher rate of water permeability penetrating the samples. Samples with 75% saturation levels (S75-C75) and (S75-C150) have a smaller size than the usual design as a consequence of not enough hydration occurring between the particles and less densification.

Table 4. Measurement of 3D printed (green part) cubic specimens

Saturation levels	Cubic dimensions (mm)	
	OPC & CAC & Li_2CO_3	OPC & CAC
S75-C75	(19.77*19.57)	(19.88*19.65)
S100-C100	(19.55*19.81)	(20.09*20.13)
S125-C125	(20.49*20.76)	(21.1*20.52)
S150-C150	(21.16*21.41)	(21.01*21.37)
S170-C170	(21.48*21.86)	(21.62*21.91)
S75-C150	(19.89*19.51)	(19.91*20.12)
S100-C200	(20.71*20.55)	(19.86*19.81)
S125-C250	(21.03*21.3)	(20.3*20.78)
S150-C300	(21.79*21.42)	(21.45*21.17)
S170-C340	(21.58*21.46)	(20.21*20.37)

The water/cement (W/C) ratio was determined by the binder/ powder mass ratio (M_b/M_p) which is available in the 3D printer software according to Eq. (2) and the results are shown in Table 5:

$$\frac{M_b}{M_p} = \frac{\rho_b . V_b}{\rho_p . V_p} \quad (2)$$

where M_b and M_p are the mass of the binder and powder, respectively; ρ_b and ρ_p are the density of binder and powder, respectively; and V_b and V_p are the volumes of binder and powder, respectively (Shakor, Sanjayan, *et al.* 2017).

Table 5. The different levels of saturation converted into water/cement ratio

Saturation level	Binder/Volume Ratio		W/C ratio
	Shell(S)	Core(C)	
S100-C200	0.244	0.244	0.310
S125-C250	0.305	0.305	0.385
S150-C300	0.366	0.366	0.460
S170-C340	0.415	0.415	0.520

The compressive strength of cubic samples is illustrated in Fig. 6. By increasing the saturation level of 3DP specimens, as a result, the compressive strength values increase gradually. This is entirely different to the results obtained by manual mixing of cementitious, which causes lower strength at high W/C ratios. All the tests were performed using a Tecnotest machine (300kN, Italy). Furthermore, the cubic samples' porosity was checked according to the Australian Standard (AS 1774.5:2014). Results show that by increasing the saturation level, total porosity decreases for 3DP specimens. Maier *et al.* (2011) stated that capillary pores and other large holes are mainly responsible for the reduction in elasticity and strength. They also found that after curing for 72 hours an intermixed crystal network developed, and this filled up the pore spaces and led to a reduced total porosity.

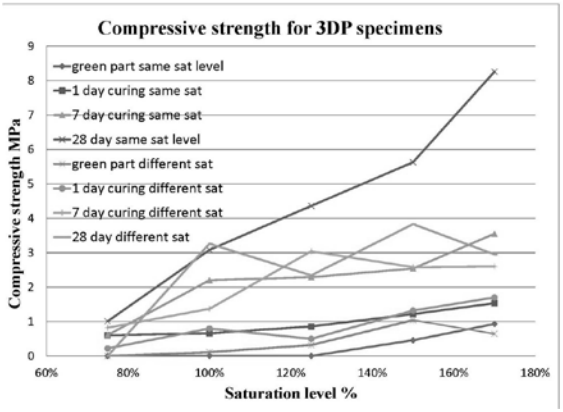

Fig. 6. Compressive strength of 3DP parts without a heating cure.

As shown in Fig. 7, the compressive strength increased when the saturation level increased, while the shell and core have similar saturation levels as explained in Table 5. At the same saturation level (shell and core) of (S100-C100-LW) 100% to (S170-C170-LW) 170% compressive strength (28 days curing) incremented from 3.08 MPa to 8.26 MPa, respectively. It is almost 37% higher than the lowest saturation level of 100%. It is linked to porosity since when porosity escalates the strength declines. Open pores affect the strength of specimens while they are being cured in water. However, there is not enough hydration and reaction between the cement particles when specimens are being printed. In addition, the CAC contains a large amount of alumina filler that leads to a demand for more water and hydration on a quicker basis (Klaus *et al.* 2016). As a result, some of the particles are unbound from the printed specimens. The maximum saturation level of Z150 is for the shell 170% and the core 340% (S170-C340) and this saturation level could not be increased. Therefore, hydration will not increase among the cement particles. Maier *et al.* (2011) claim that the limited amount of water released from the head of the printer and the process did not provide enough strength for the specimen. Nevertheless, the 3DP samples have less strength than the hand mixed samples, as shown in Fig. 6 and 7.

From the Fig. 6, it is noticeable for different saturation levels, the optimum strength is (8.26MPa) at a saturation level of (S170-C170-LW) in 3DP samples for 28 days. This may be due to the level of porosity between particles being higher where the

saturation level is low. It is slightly different with other saturation levels. As shown in Fig. 7, lower water ratios for hand mixed samples result in higher strength. The tests have been applied for all categories of different saturation levels after finding the ratio of saturation levels is converted to the water/cement ratio.

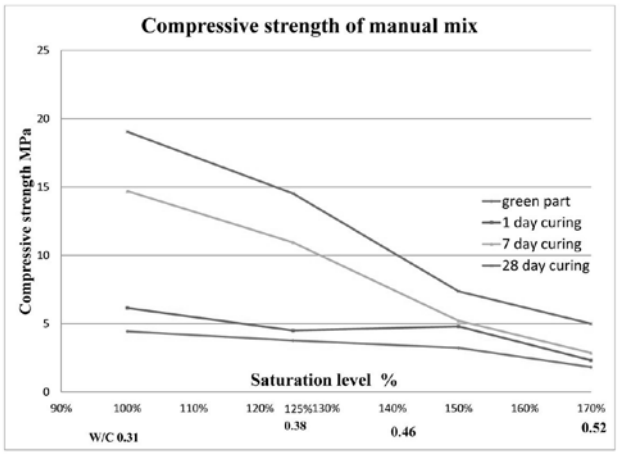

Fig. 7. Compressive strength of manual mix cementitious materials

As illustrated in Fig. 7 at saturation level S100-C200 in 3DP which is equal to W/C 0.31, the highest compressive strength can be obtained (19.05MPa). According to (Feng, Meng, Chen, *et al.* 2015) 3DP directions has an impact on compressive strength when printing samples in different directions. They contend that the speed of the printer in X-direction is faster than other directions. Further, the time of printing adjacent layers at the Y-direction is shorter than printing adjacent layers in the Z-direction. The level of bond between two parts of the particles is thereby higher in a shorter print time, resulting in higher strength in a continuous strip rather than the strip in between. As shown in Fig. 8, in this study the load is parallel to the Z-direction when this load is applied, cracks pass through the interior strip (i.e. vertical) direction. 3DP cubes also find the lateral sides get spalled and ruptures occur due to crushing.

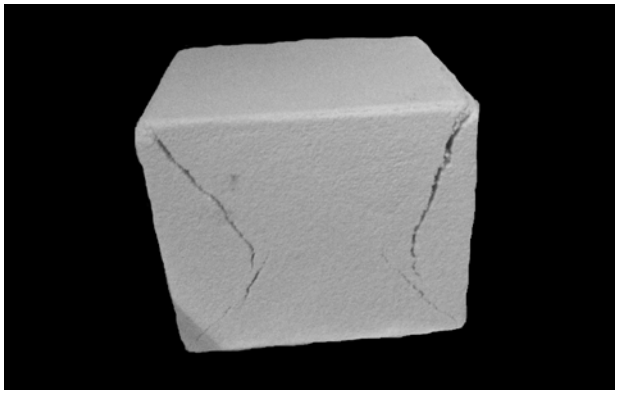

Fig. 8. Diagonal crack inside the Z-powder specimen (50×50) mm.

After curing in water, part of the samples is dried in the oven. The highest compressive strength was recorded (14.68±0.43 MPa). This was compared to other recorded samples that were cured without drying at high temperature was (4.81±0.86 MPa). These are explained in more detail in Fig. 9. The 3DP sample (S170C340-SH) had the highest result in compressive strength when cured for 28 days in water and then dried for about one hour at (40°C) in the furnace. The tests were conducted in the laboratory with samples which were dried in the furnace (Vtech, XU 225) at 40°C for approximately one hour and then left to cool to room temperature. Goto & Roy (1981) claimed that Tricalcium Silicate (C_3S) becomes larger in size at high cured temperature than cured at a lower temperature in an early age. Fig. 10 showed that the flexural strength in the X-direction had the highest strength (approximately 6.21MPa) due to the fact of less number in layers to construct in this direction compared to the other directions (axes).

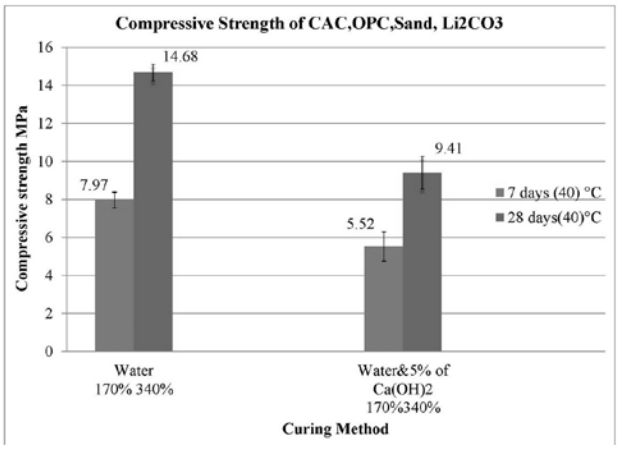

Fig. 9. Compressive strength of mortar mix 3DP materials after dried in an oven for S170C340

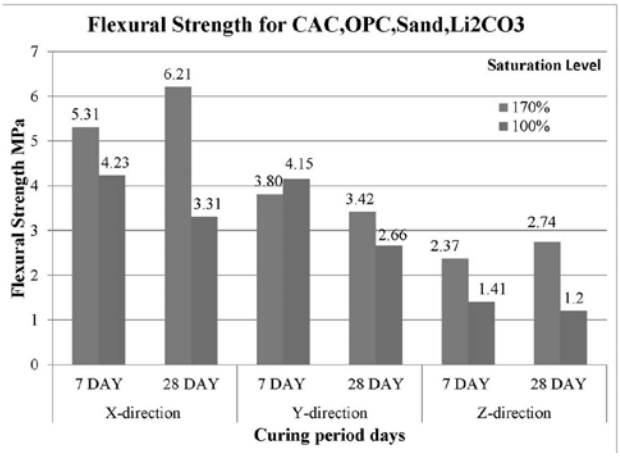

Fig. 10. Flexural strength of cementitious prism in different directions (X, Y, and Z) and saturation levels for 170% and 100% saturation levels

According to Farzadi *et al.* (2014), the layer thickness and printing orientation affect the optimal conditions of the maximum green strength and

dimensional accuracy. They claimed that printing in the X-direction was the most notable orientation for constructing a 3D model. This was due to the acceptable coincidences between the layers in this direction where the movement is parallel to the printer head. Furthermore, Castilho *et al.* (2011) stated that the 3DP scaffold stiffness decreases when the number of elementary units (layers) increases. The samples with the lowest porosity between the particles and adjacent layers allowed for better bonds to create a form at the ideal time. Another study suggests that the best results for the 3DP sample can be achieved (with respect to either the flexural or compressive strength) with a proper thickness of approximately 0.1mm (Vaezi & Chua 2011). In the present study, a similar thickness was applied. Vaezi & Chau's experimental work has found that, with the same printing layer thickness, increasing the binder saturation level from 90% to 125% increases the sample's flexural and tensile strengths. It also reduces the surface consistency and dimensional accuracy, which is proved similar outcomes in this presented study. To evaluate the flexural strength of printed specimens, manually mixed samples were arranged with the same dimensions and compacted well by shake table. It was noted that flexural strength at a saturation level of (S125C250) was recorded as the highest result approximately 9.77 MPa (see Fig. 11). Therefore, the manually mixed outcomes were higher than the 3D printed samples, due to good vibration in the normal mix. The specimens were produced in accordance with printer constraints, similar to those of (Feng, Meng & Zhang 2015) who conducted their samples in a similar way.

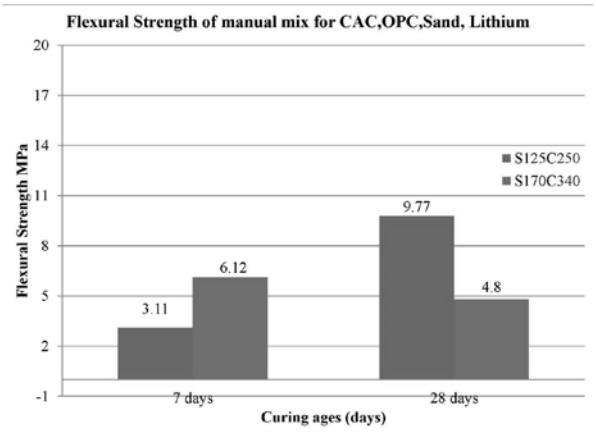

Fig. 11. Flexural strength for manual mortar mix materials for saturation levels S125C250& S170C340

Figure 4 illustrates the outcome of porosity of 3D printed samples at different and similar saturation levels when using lithium carbonate and without lithium carbonate. The lowest level of porosity was recorded at the different saturation levels of samples at S170-C340-LW. It is Illustrated in Fig. 12 which is the test performed using Scanning Electronic Microscope (SEM). Therefore, it exhibits the porosity between particles of the printed specimen. Plate-like large crystal growths occurred which have some other unreacted particles on the surface of the specimens. Moreover, it can be seen that there are deep holes and incohesive particles on SEM Fig. 12. It is evident that hydration was not completed between the cement particles.

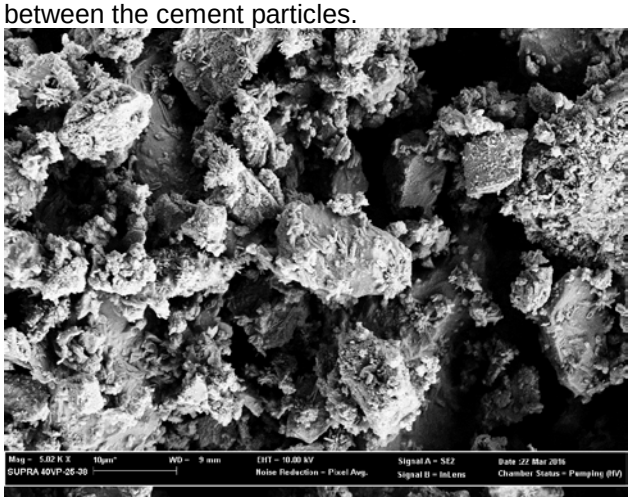

Fig. 12. SEM image of 3D printed samples, (10 µm).

The 3D profiling assisted to detect the porosity of specimens. As shown in Fig. 14, the different saturation levels of specimens with different magnifications were tested to explore the porosity and surface roughness of the samples.The test employed technique 3D profile Veeco (Dektak) with the following magnifications: 2.5x and 50x. The clear porosity and haphazard surface shape of the 3D-printed specimens are visible in Fig. 15. The samples on the same spot were tested in the side layer (Z-direction, the vertical direction in 3DP) for the green part and in water cured samples, Fig. 13. However, after 7 days the in water cured samples were examined by the 3D profile and it showed pit (porous holes) on their surface area. The topographical shape of height distributions changed dramatically. It shows the value of skewness (*Ssk*) after curing and most samples have positive signs, which mean many high spikes appeared on the surface. The (*Ssk*) parameter correlated with load bearings and porosity. According to Petzing *et al.* (2010) the *Ssk* is zero when the height distribution has a symmetrical surface. This is validated by the centre line for symmetrical and unsymmetrical purposes. So the direction of skew is differentiated above the mean line (negative skew) or below the mean line (positive skew). Figures 14 and 15 show that the samples released and left many particles. Therefore, pit (porous holes) clearly appeared on the surface of cured samples in water.

Generally, the 3DP process is complex and many studies continue to focus on different materials formulation. In general, the powder consisted of; CAC passing sieve 150 µm and OPC does not achieve enough strength in 3DP specimens. One of the reasons for this may be the water (binder) of the printer is not quite enough to hydrate all particles of

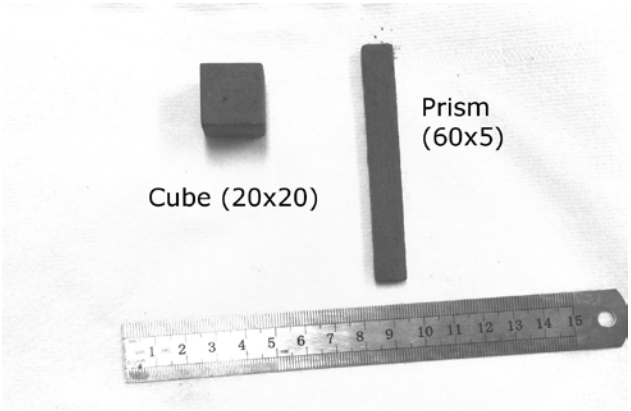

Fig. 13. Printed cube and prism via inkjet printer (3D Zprinter ®150) (dimensions are in mm)

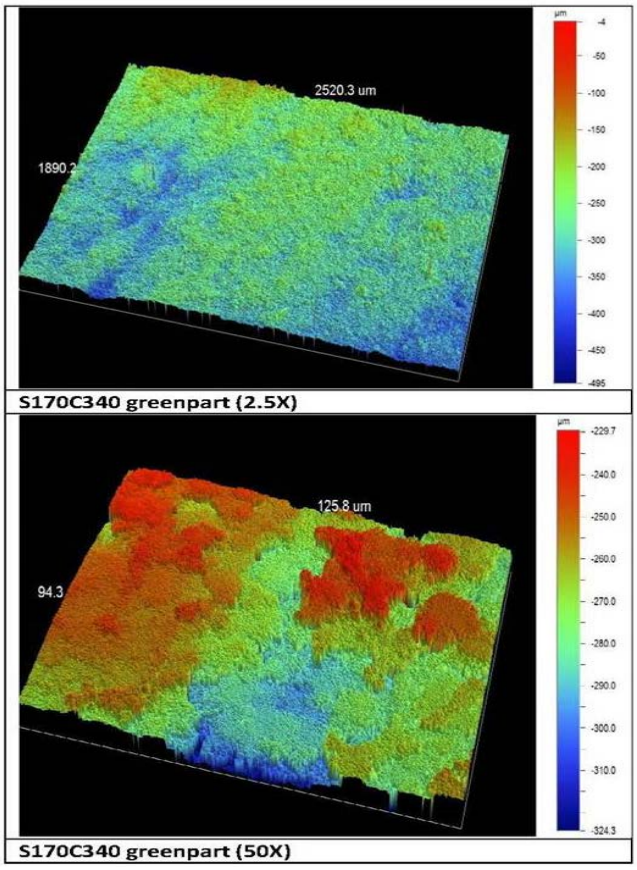

Fig. 14. Some 3D profiling image for 3D printed samples (green part)

the material. The morphology of the particles and presence of interparticle pores could be another reason. The fine particles of cement may provide an additional reason, and according to (Kirchberg *et al.* 2011) fine particles increase the contact angle and reduce the powder's wettability. Moreover, the binder was also not pure water, as it included about 5~10% of polyvinyl alcohol or glycerol (humectant) or methanol (20% volume of binder). The research of Sun *et al.* (2013) used nozzles of 30 Micron to print the layers of ink on the glass to control the ink solidification, and it used solvent materials in water (boiling point 100ºC) evaporation during the printing

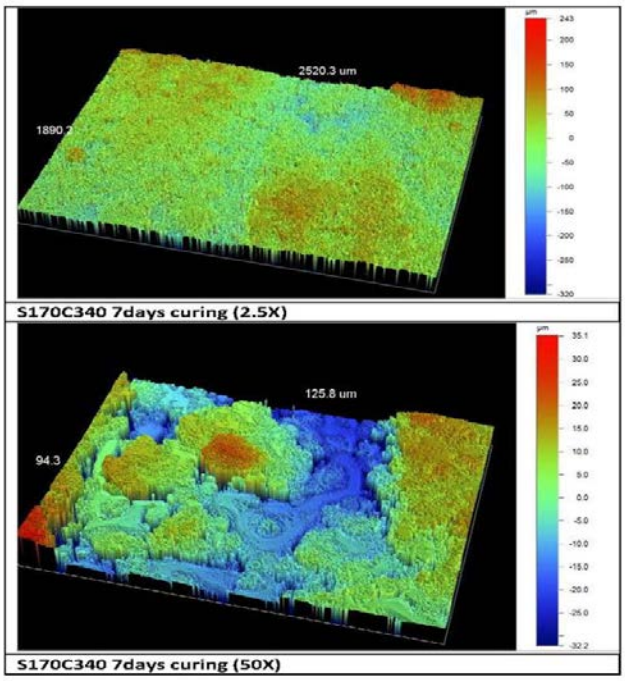

Fig. 15. Some 3D profiling image for 3D printed samples (after 7days curing).

process to induce partial solidification, while ethylene glycol (b.p. 197.3ºC) and glycerol (b.p. 290ºC) acted as humectants. That humectant is not suitable for use as a mixed water-based binder because it reduces the compressive strength of cementitious materials.

3.2 Durability of the 3DP specimens

In general, durability is the ability of materials to resist the different environments for long period without significant deterioration. For the concrete durability is dependent on five major factors including; curing, compaction, cement content, permeability and cover. These factors are discussed in more details in the following sections.

The curing or post-processing plays a major role in the durability of the printed specimens. Moreover, the curing process for the ordinary concrete is commonly keeping concrete in a moist environment or into the water. However, for the 3D printed specimens, we use different methods such as keeping in water only or curing in water for 28 days and then dried at 40°C in an oven for an hour. The results of these experiments are explained in the results and discussion (material composition) section, which shows the main enhancement in the mechanical properties when it has been dried in the oven. Consequently, the compressive strength increases twice than the normal curing specimens.

In addition, a proper compaction in the concrete or vibration increases the density and durability of the concrete. This function is unattainable in the 3DP application which is only spread the powder by a

roller. The spreading powder by the roller has a slight compaction on the bedded powder, this process is called in-process bed powder preparation(Zhou *et al.* 2014). The density of the 3DP cementitious mortar has been measured. It has been observed which has a lesser density than the normal concrete due to lack of vibration and high porosity among particles. The density of the 3DP part is 1764±60 kg/m^3, see Table (6), as it is noticeable normal concrete has density 2400 kg/m^3.

Table 6. Detailed measurement of the printed specimens for the different saturation levels (S170C340)

Sample description	Curing condition	Dimensions (mm)		Weight (gram)	
		7 days	28 days	7 days	28 days
S170 C340	Water(40°C)	(20.94X 20.64)	(21.53 X 22.07)	15.85	16.55

Another factor which affects the durability is the cement content. The comprised materials of the printed structure are contained a high amount of cement and a limited amount of sand (5% of cement weight). The mechanism of building the printed specimens is totally different compared to the ordinary concrete. The nozzles of the printer are locating specific areas to drop water droplet on the bedded powder. Thus, the entire part of the printed specimen could not be able to be saturated sufficiently. Furthermore, the mechanical properties of the 3DP specimens have weaker properties comparing to the normal concrete. This needs an extra investigation to improve the 3DP specimens to obtain higher mechanical properties.

The permeability is another factor which should be considered into account for the 3DP specimens. This topic is linked to the porosity of the specimens which has been explained in the section of (Preparation of the specimens). Minimum porosity level for the 3DP specimens is about 62% which means that the printed specimen has a permeable medium. As a result, the post-processing has a major influence on improving the 3DP permeability. The curing process in 3DP has a different technique which depends on the type of materials. For instance, for the Zpowder samples usually we use infiltration for the curing purposes or we cure in an oven for few hours. Infiltration method consists of applying a specific resin on the printed part in order to provide higher strength and improve the mechanical properties. In addition, the Zcorp company provides several post-processing products such as wax, resins, epoxy, etc. This production improves specific characterization of the specimens such as strength, durability, and colour vibrancy, see Fig. 16.

Figure 17 clearly shows the fluctuation of porosity versus compressive strength while increasing the w/c ratio, the compressive strength increases slightly as well. On the other hand, when porosity reduced, the compressive strength has been increased slightly which is the rational result. Having a high rate of porosity makes the concrete strength weaker.

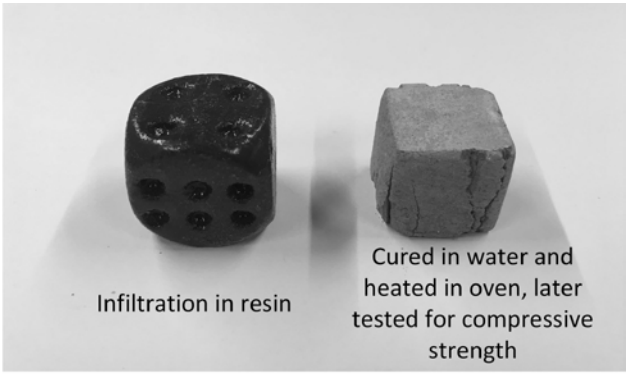

Fig. 16. 3DP specimens are cured by different agents

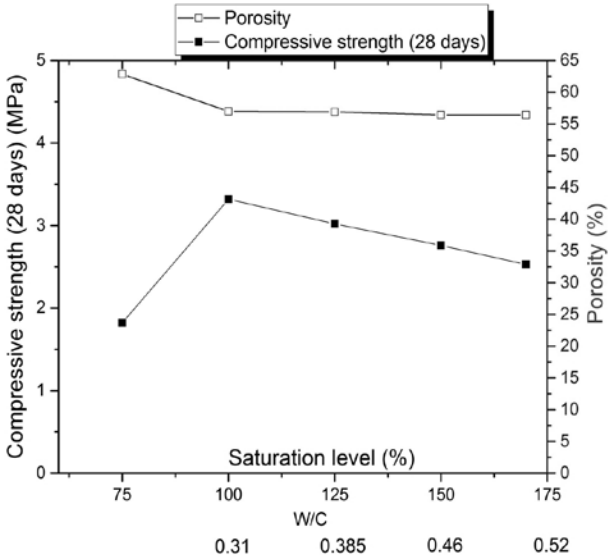

Fig. 17. Schematic illustration of porosity vs. compressive strength

Generally, 3DP specimens do not observe any shrinkage cracks in the specimens. To better understanding, further work needs to be done to check the microcracks inside the samples. Morphology of the 3DP specimens has been studied for the purpose of obtaining particle size observation. Fig. 18 showed the morphology of the powders before printing, it displayed that the cementitious powder has a heterogeneous arrangement compare to the Zpowder. Therefore, both powders would have a different percentage of porosity and different microstructure composition.

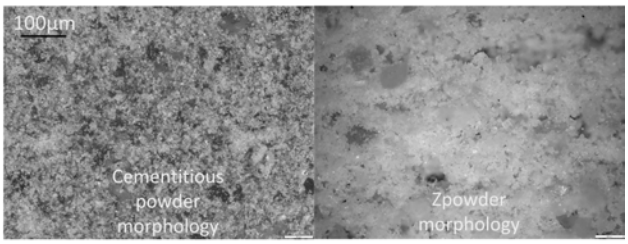

Fig. 18. Morphology of cementitious powder and Zpowder

4.0 CONCLUSIONS

An approach has been developed to use a new material instead of the Z-powder 3DP (Z-corp 150). Lately, 3DP has been used for a variety of purposes so in this paper 3D printing was applied specifically targeting civil engineering applications. The study was implemented on Z-Corp 150 with the Z-printer powder replaced with equivalent powder blend that has similar properties. The results indicated that increasing the saturation levels, resulted in increased compressive strength when the shell and core of samples had the same saturation level, i.e. 100% saturation level (S100-C100). The maximum saturation level of 170% recorded the highest compressive strength. While in different saturation levels of shell and core (e.g. core being twice as saturated as the shell), in this saturation level the optimum compressive strength is at S150-C300. Moreover, it is generally agreed that porosity influences the compressive strength of cementitious materials, with more pores meaning there is less toughness. In addition, cubic specimens for manual mix design (hand mix) exhibit different properties. Thus, by increasing the water/cement ratio, the strength of cement will reduce. The reverse will also be the case for the 3DP, the high saturated liquid will obtain high mechanical strength. Different structures could be produced using these types of cementitious (CAC&OPC) materials. The 3DP could also print in different angles and directions so that the mechanical strength and amount of porosity of the printed specimen could be optimised in the design phase, and thus potentially reduced dramatically. Furthermore, the durability of the printed element has been conducted briefly in the presented study.
Obtaining reasonable strength in this study for some specimens could bring about the production of large structural elements. This study also describes the influence of various parameters and how they can affect the quality of the sample. Moreover, the study presented some experiments on producing a higher compressive strength when curing in a furnace while using the CAC & OPC powder. The compressive strength under different curing conditions and drying at high temperatures was also discussed.

Acknowledgement

The author's are greatful to the Centre for Sustainable Infrastructure at the Swinburne University of Technology for their technical support.

References

3DSystems 2012, ' ZPrinter 150 / ZPrinter 250 Overview'.

Asadi-Eydivand, M., Solati-Hashjin, M., Farzad, A. & Abu Osman, N.A. 2016, 'Effect of technical parameters on porous structure and strength of 3D printed calcium sulfate prototypes', *Robotics and Computer-Integrated Manufacturing*, vol. 37, pp. 57-67.

Buswell, R.A., Soar, R., Gibb, A.G. & Thorpe, A. 2007, 'Freeform construction: mega-scale rapid manufacturing for construction', *Automation in construction*, vol. 16, no. 2, pp. 224-31.

Castaneda, E., Lauret, B., Lirola, J. & Ovando, G. 2015, 'Free-form architectural envelopes: Digital processes opportunities of industrial production at a reasonable price', *Journal of Facade Design and Engineering*, vol. 3, no. 1, pp. 1-13.

Castilho, M., Pires, I., Gouveia, B. & Rodrigues, J. 2011, 'Structural evaluation of scaffolds prototypes produced by three-dimensional printing', *The International Journal of Advanced Manufacturing Technology*, vol. 56, no. 5-8, pp. 561-9.

Farzadi, A., Solati-Hashjin, M., Asadi-Eydivand, M. & Abu Osman, N.A. 2014, 'Effect of layer thickness and printing orientation on mechanical properties and dimensional accuracy of 3D printed porous samples for bone tissue engineering', *PLoS One*, vol. 9, no. 9, p. e108252.

Farzadi, A., Waran, V., Solati-Hashjin, M., Rahman, Z.A.A., Asadi, M. & Osman, N.A.A. 2015, 'Effect of layer printing delay on mechanical properties and dimensional accuracy of 3D printed porous prototypes in bone tissue engineering', *Ceramics International*, vol. 41, no. 7, pp. 8320-30.

Feng, P., Meng, X., Chen, J.-F. & Ye, L. 2015, 'Mechanical properties of structures 3D printed with cementitious powders', *Construction and Building Materials*, vol. 93, pp. 486-97.

Feng, P., Meng, X. & Zhang, H. 2015a, 'Mechanical behavior of FRP sheets reinforced 3D elements printed with cementitious materials', *Composite Structures*, vol. 134, pp. 331-42.

Goto, S. & Roy, D.M. 1981, 'The effect of w/c ratio and curing temperature on the permeability of hardened cement paste', *Cement and Concrete Research*, vol. 11, no. 4, pp. 575-9.

Kirchberg, S., Abdin, Y. & Ziegmann, G. 2011, 'Influence of particle shape and size on the wetting behavior of soft magnetic micropowders', *Powder Technology*, vol. 207, no. 1–3, pp. 311-7.

Klaus, S.R., Neubauer, J. & Goetz-Neunhoeffer, F. 2016, 'Influence of the specific surface area of alumina fillers on CAC hydration kinetics', *Advances in Cement Research*, vol. 28, no. 1, pp. 62-70.

Lin, X., Zhang, T., Huo, L., Li, G., Zhang, N. & Liao, J. 2015, 'Preparation and Application of 3D Printing Materials in Construction'.

Lipson, H. & Kurman, M. 2013, *Fabricated: The new world of 3D printing*, John Wiley & Sons.

Lloret, E., Shahab, A.R., Linus, M., Flatt, R.J., Gramazio, F., Kohler, M. & Langenberg, S. 2015, 'Complex concrete structures: Merging existing casting techniques with digital fabrication', *Computer-Aided Design*, vol. 60, pp. 40-9.

Maier, A.-K., Dezmirean, L., Will, J. & Greil, P. 2011, 'Three-dimensional printing of flash-setting calcium aluminate cement', *Journal of materials science*, vol. 46, no. 9, pp. 2947-54.

Michele, L. & Emanuel, S. 2003, 'Improved surface finish in 3D printing using bimodal powder distribution', *Rapid Prototyping Journal*, vol. 9, no. 3, pp. 157-66.

Miyanaji, H., Zhang, S., Lassell, A., Zandinejad, A.A. & Yang, L. 2016, 'Optimal Process Parameters for 3D Printing of Porcelain Structures', *Procedia Manufacturing*, vol. 5, pp. 870-87.

Petzing, J.N., Coupland, J.M. & Leach, R.K. 2010, 'The measurement of rough surface topography using coherence scanning interferometry'.

Shakor, P., Renneberg, J., Nejadi, S. & Paul, G. 2017, 'Optimisation of Different Concrete Mix Designs for 3D Printing by Utilizing Six Degrees of Freedom Industrial Robot', paper presented to the *34th International Symposium on Automation and Robotics in Construction*, Taipei, Taiwan

Shakor, P., Sanjayan, J., Nazari, A. & Nejadi, S. 2017, 'Modified 3D printed powder to cement-based material and mechanical properties of cement scaffold used in 3D printing', *Construction and Building Materials*, vol. 138, pp. 398-409.

Sun, K., Wei, T.S., Ahn, B.Y., Seo, J.Y., Dillon, S.J. & Lewis, J.A. 2013, '3D Printing of Interdigitated Li-Ion Microbattery Architectures', *Advanced Materials*, vol. 25, no. 33, pp. 4539-43.

Vaezi, M. & Chua, C. 2011, 'Effects of layer thickness and binder saturation level parameters on 3D printing process', *The International Journal of Advanced Manufacturing Technology*, vol. 53, no. 1-4, pp. 275-84.

Wegrzyn, T.F., Golding, M. & Archer, R.H. 2012, 'Food Layered Manufacture: A new process for constructing solid foods', *Trends in Food Science & Technology*, vol. 27, no. 2, pp. 66-72.

Zhou, Z., Buchanan, F., Mitchell, C. & Dunne, N. 2014, 'Printability of calcium phosphate: calcium sulfate powders for the application of tissue engineered bone scaffolds using the 3D printing technique', *Mater Sci Eng C Mater Biol Appl*, vol. 38, pp. 1-10.